A study of interlayer exchange coupling in a Co/Cr/Co trilayer using transmission electron microscopy

A. C. Daykin,[a] J. P. Jakubovics,[b] and A. K. Petford-Long
Department of Materials, University of Oxford, Parks Road, Oxford OX1 3PH, United Kingdom

(Received 20 January 1997; accepted for publication 20 May 1997)

Magnetic induction maps from a sputter-deposited Co/Cr/Co trilayer have been obtained at different points of the hysteresis cycle, using a conventional transmission electron microscope. The sample shows hysteresis, with nearly parallel alignment of the magnetization in the two Co layers at remanence, but areas of antiparallel alignment developing in reverse fields. Such areas occur in similar positions at opposite points of the hysteresis loop. The strongly correlated domain patterns seen in opposite field directions suggest that the interlayer exchange coupling varies spatially. The parallel alignment observed at remanence suggests the presence of an energy barrier that needs to be overcome before antiparallel alignment can be formed. This conclusion is supported by observations of the film in a demagnetized state. © *1997 American Institute of Physics.* [S0021-8979(97)00217-X]

I. INTRODUCTION

Magnetic multilayer films (MLFs) composed of thin ferromagnetic layers separated by nonmagnetic or antiferromagnetic spacer layers exhibit several interesting properties not found in bulk ferromagnetic elements or alloys. Some MLFs, such as those in which the magnetic layers are Fe or Co and the nonmagnetic layers are Cr or Cu, show unusually large changes in resistance when a magnetic field is applied, for certain thicknesses of the spacer layers.[1,2] This effect, called giant magnetoresistance (GMR), occurs when the moments of the adjacent magnetic layers are aligned antiparallel in the absence of an applied magnetic field, but switch to a parallel orientation when a field is applied. The change of resistance associated with the change in the alignment of the magnetic moments arises because the electrons have a shorter mean free path between scattering events when they travel through two magnetic layers in which the magnetic moments are misaligned.[3–5] The GMR effect has now been observed in a wide range of systems. Magnetic MLFs exhibiting GMR are potentially useful as magnetic field sensors, such as read heads in magnetic recording systems. However, to exploit the GMR effect for practical applications, the devices must change their resistance substantially in small applied fields. Unfortunately, because of the complicated relationship between the structure and properties of these MLFs, it is difficult to predict the component materials and growth procedures that will produce MLFs with useful properties. A further problem is that cost-effective devices need to be mass produced by fast growth techniques, such as sputtering, which tend to produce MLFs with very complicated microstructures.

The magnetic moments in adjacent magnetic layers of a multilayer stack are coupled by exchange interactions across the spacer layers. The magnitude and sign of the exchange interaction oscillate as functions of the thickness of the spacer layer.[2] Thus at certain thicknesses of the spacer layer the interlayer exchange coupling is ferromagnetic, while at other thicknesses it is antiferromagnetic. The period of oscillation from ferromagnetic to antiferromagnetic coupling for Co/Cr MLFs is[2] approximately 2.1 nm, but more rapid oscillations with a period of two monolayers ($\approx$0.3 nm) have also been observed for Fe/Cr/Fe trilayers grown by molecular beam epitaxy.[6,7] Consequently, the interlayer exchange coupling in magnetic MLFs is strongly dependent on variations in thickness of the spacer layer, and on interface roughness. Because of the fact that sputter deposition results in polycrystalline samples with a very small grain size, it is known that parameters such as the layer thickness and interface quality can vary locally on a fine scale, resulting in local variations in the interlayer exchange coupling.

In order to study this effect, we have carried out a study of trilayer systems. Trilayers have fewer interfaces than MLFs, and thus they can be used as model systems for studies of interlayer coupling. There are several methods for such studies, but most of them only provide information about the coupling averaged over the whole trilayer specimen. In order to study variations in coupling between different areas of the trilayer film, the most useful technique is to image the magnetic domain structure. However, even such relatively simple systems can have complicated magnetic domain structures, and the interlayer exchange coupling can best be studied by observing changes in domain structure as a function of applied fields. We have therefore performed a series of *in situ* magnetizing experiments using a recently developed technique based on the Foucault method of Lorentz microscopy, which enables differential phase contrast images to be obtained at high spatial resolution in a conventional transmission electron microscope (TEM).[8,9] The technique can be used in combination with *in situ* magnetizing.

II. EXPERIMENTAL METHODS

Co/Cr/Co trilayers were deposited directly onto a carbon film on a TEM grid by magnetron sputtering at an Ar pressure of approximately 3.0×10^{-3} Pa. The chamber pressure

[a]Current address: Structural Metals Centre, DERA Farnborough, Farnborough, Hants GU14 6TD, UK.
[b]Electronic mail: john.jakubovics@materials.oxford.ac.ok

prior to deposition was approximately 6.5×10^{-6} Pa. In all trilayers, the thickness of the two Co layers was approximately 10 nm, but that of the Cr spacer layer was different in different trilayers. All the results presented in this article are for a trilayer with a Cr layer thickness of approximately 1 nm. The samples were studied in a JEOL 4000EX TEM operated at 400 kV, and fitted with an AMG40 low-field objective pole-piece, which ensures that the specimen is held in a position free from strong magnetic fields. A side-entry specimen holder has been constructed, which enables the specimen to be tilted by $\pm45°$ and rotated by 300°. It is fitted with a pair of Mu-metal-cored magnetizing coils on opposite sides of the specimen, which can produce a field along the axis of the specimen holder, variable up to ±370 Oe. The field varies by less than 10% over the volume of the specimen, and its residual value with no current passing through the coils is less than 1 Oe. The misalignment introduced by the applied field can be corrected for fields up to 100 Oe by tilting the electron beam either above or below the specimen.

The magnetic domain structure can be observed in the TEM in images taken with the specimen slightly out of focus (Fresnel images),[10–12] in which the positions of the domain walls appear as bright or dark lines, or with the objective aperture slightly displaced from its central position (Foucault images),[11–14] in which electrons that have passed through certain domains are obstructed by the aperture, causing those domains to appear dark. In the present work, images were recorded using a variation of the Foucault technique.[15,16] In this variation, the focal length of the objective lens is increased until the back-focal plane coincides with the plane of the selected-area aperture. A highly magnified diffraction pattern can then be observed on the viewing screen, in which the effects of the deflection of parts of the transmitted beam caused by the magnetic induction can easily be seen. Foucault images are obtained by displacing the selected-area aperture from its central position.[16]

The intensity distribution in a single Foucault image does not provide an accurate map of the magnetic induction distribution. However, by combining two series of Foucault images taken with small incremental tilts of the incident illumination, two component maps, $B_{xi}(x,y)$ and $B_{yi}(x,y)$, of the magnetic induction integrated along the electron trajectory, $\mathbf{B}_i(x,y)$, can be produced, which can then be combined to produce a map of $\mathbf{B}_i(x,y)$.[8] The method is equivalent to that used by Chapman in that both provide differential phase contrast images.[17–19] The Chapman method is however normally implemented in dedicated scanning TEMs,[20] or a TEM with a scan unit,[21] whereas our method is implemented in a conventional TEM.

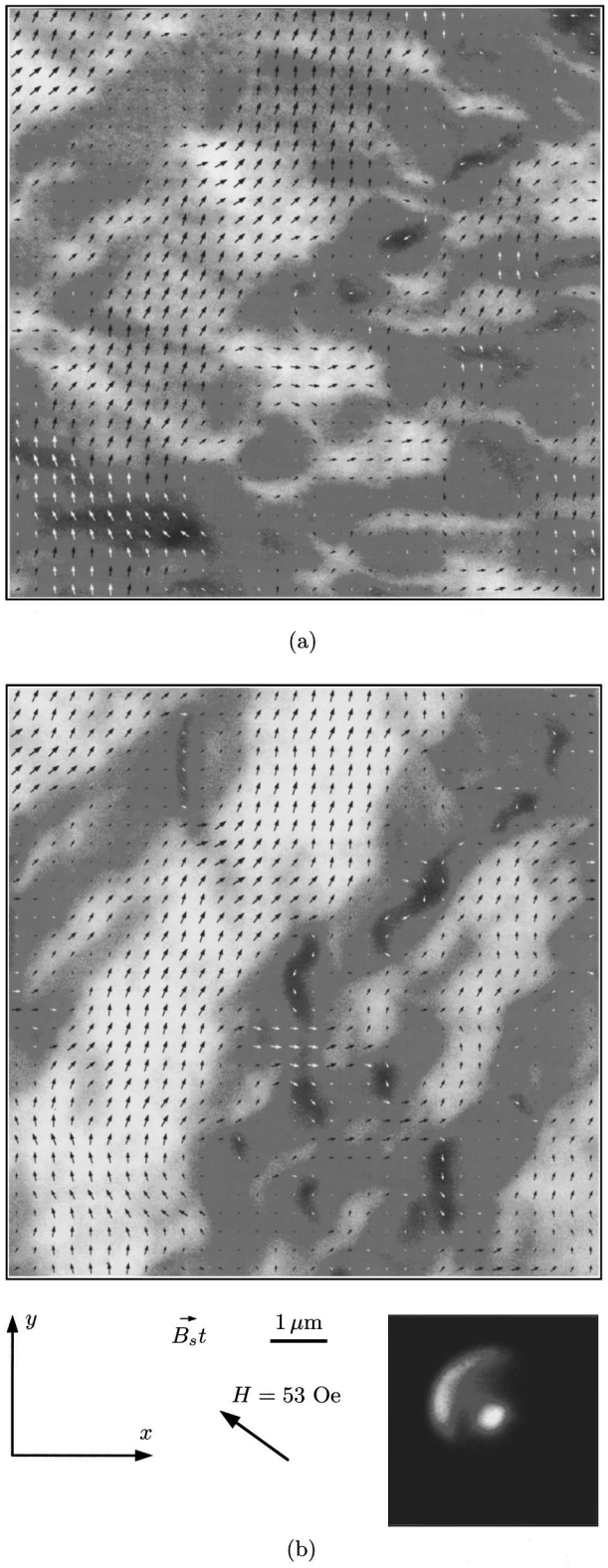

FIG. 1. Maps of $\mathbf{B}_i(x,y)$, the magnetic induction averaged along the electron trajectory, for a $Co_{10\ nm}/Cr_{1\ nm}/Co_{10\ nm}$ trilayer in a magnetic field of 53 Oe. Maps of the components $B_{xi}(x,y)$ and $B_{yi}(x,y)$ are shown in (a) and (b), respectively. The arrow labeled $B_s t$ in (b) corresponds to $\mathbf{B}_i$ in a saturated region, and (b) also shows a high-magnification diffraction pattern.

III. RESULTS

Figures 1(a) and 1(b) show maps of two orthogonal components $B_{xi}(x,y)$ and $B_{yi}(x,y)$ respectively, of $\mathbf{B}_i(x,y)$ taken from a $Co_{10\ nm}/Cr_{1\ nm}/Co_{10\ nm}$ trilayer film in a field $H\approx53$ Oe applied in the direction shown. The superimposed gray-scale in each figure indicates the magnitude of the component being mapped, white and black corresponding to a large positive and large negative value of that component, respectively. Superimposed on each figure is a vector map of $\mathbf{B}_i(x,y)$. The length of the arrows of this vector map is proportional to $|\mathbf{B}_i(x,y)|$, and the arrows point in the direction

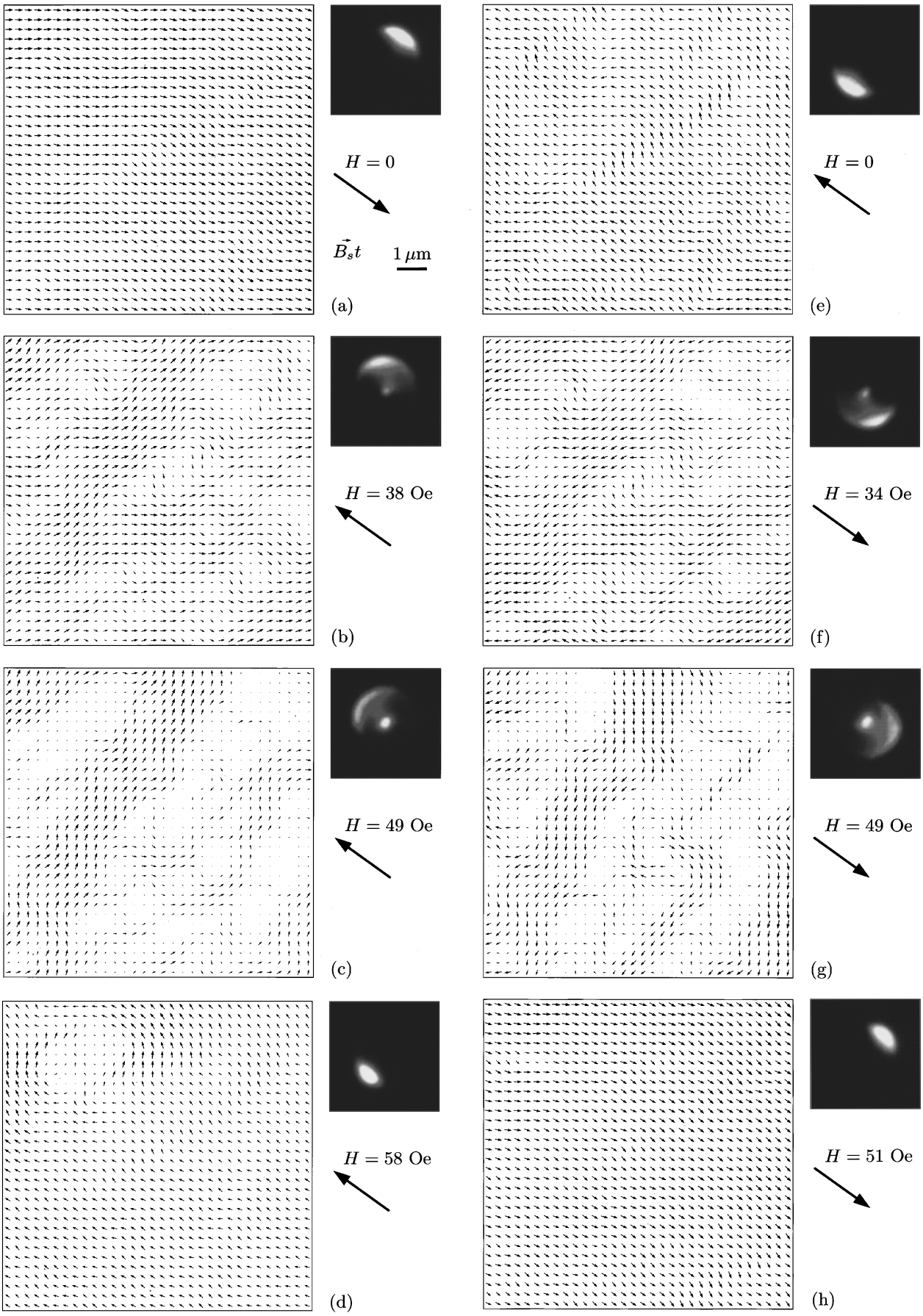

FIG. 2. Maps of $\mathbf{B}_i(x,y)$ for the same area of a $Co_{10\,nm}/Cr_{1\,nm}/Co_{10\,nm}$ trilayer as shown in Fig. 1, in various applied fields.

of $\mathbf{B}_i(x,y)$. The arrows are black or white according to whether the component being mapped is positive or negative. Figure 1(b) also shows a high-magnification diffraction pattern of the region of reciprocal space in which the Lorentz scattering occurs.

The maps shown in Fig. 1 were produced as part of a series of images taken at different values of applied field around a hysteresis cycle. A field $H \approx 370$ Oe was first applied and removed, and a map was recorded in the remanent state. A gradually increasing field was then applied in the opposite direction, and maps were recorded for various values of H up to 59 Oe. The field was then further increased to 370 Oe and decreased to zero before recording the next map. Further maps were recorded with the field applied in the direction of the original saturating field, for various values of H up to 51 Oe. Eight of these maps (in the form of arrow maps only) are shown in Fig. 2. To the right of each map is a large arrow indicating the direction of the applied field, with the magnitude of the field also given. In the case of the two remanent states, (a) and (e), with $H=0$, the arrow points in the direction of the previously applied saturating field. The value of $\mathbf{B}_i$ in a saturated region is indicated by the small horizontal arrow labeled $B_s t$ to the right of (a). To the right of each map, the corresponding high-magnification diffraction pattern is included, showing the region of Lorentz scattering.

Figure 2(a) shows the initial remanent state. The magnetic moments are aligned approximately in the direction of the field previously applied to saturate the film, although some magnetization ripple is visible. The arrows throughout the area are large, indicating parallel alignment of the magnetization in the two Co layers. In the corresponding high-magnification diffraction pattern an arc-shaped Lorentz deflection spot is seen. The bright parts of this pattern correspond to the deflection of the electrons that have passed through the two Co layers magnetized in the same direction. The arc shape is due to the magnetization ripple, the angle subtended by the arc being equal to the angular spread of the ripple.

As the field is increased in the opposite direction, a domain structure begins to develop. Figure 2(b) shows the same area in a field $H \approx 38$ Oe. Areas of the sample can be seen in which the arrows are small, as well as other areas with large arrows. It was shown by tilting the sample that there is no significant component of magnetic induction perpendicular to the film plane. The small arrows therefore indicate areas in which the magnetization directions in the two Co layers lie antiparallel. In the diffraction pattern two spots are apparent, one at the center of the pattern, originating from regions of the sample with a very small $|\mathbf{B}_i|$ (small arrows, antiparallel moments), and the other, which is arc-shaped, originating from the regions in which $|\mathbf{B}_i|$ is large. The arc shape again arises because of the presence of magnetic ripple in the parallel-aligned regions. Figure 2(c) shows a map of the same area in $H \approx 49$ Oe, with an increased area containing antiparallel alignment.

In $H \approx 58$ Oe [Fig. 2(d)] the film switches to a state in which the moments in the two Co layers are aligned nearly parallel. There is still, however, a small region in the top left of the image in which the moments are aligned antiparallel. In the subsequent remanent state [Fig. 2(e)], the alignment of the magnetization in the two Co layers remains parallel, but pronounced magnetization ripple is present. As an increasing field is applied in the opposite direction, a domain structure forms in which there are again distinct areas of antiparallel and parallel alignment. By comparing the domain images in Figs. 2(b) and 2(c) with those in Figs. 2(f) and 2(g), respectively, it can be seen that there is a strong correlation between the areas of parallel and antiparallel alignment in similar fields applied in opposite directions [$H \approx 38$ Oe and 34 Oe in (b) and (f), respectively, and $H \approx 49$ Oe in (c) and (g)].

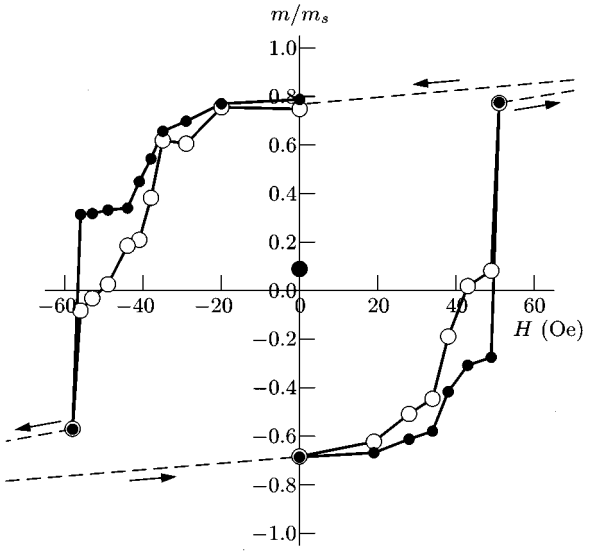

FIG. 3. A hysteresis loop for the area of the sample shown in Figs. 1 and 2 constructed from 19 maps of the magnetic induction collected in different applied magnetic fields. The full and empty circles represent the magnetic moment of the film, and its component in the direction of H, respectively. The dashed lines indicate the parts of the magnetization cycle during which maps of $\mathbf{B}_i$ were not recorded. The extra point near the origin corresponds to the demagnetized state (see Fig. 4).

From each map of $\mathbf{B}_i(x,y)$, the average induction in any particular direction can be determined by integrating the component of the induction in that direction over the field of view. Figure 3 shows two hysteresis loops for the area of the Co/Cr/Co trilayer shown in Figs. 1 and 2. The full circles represent the magnetic moment of the film at each value of H, whereas the empty circles represent the component of the magnetic moment in the direction of H, the positive direction being chosen as the one in Figs. 2(b)–2(d). The dashed lines indicate schematically the parts of the magnetization cycle during which magnetic induction maps were not recorded, and the arrows show the direction in which the magnetization loop was traversed. The extra point near the origin corresponds to the demagnetized state (see Sec. IV and Fig. 4).

IV. DISCUSSION

The equilibrium distribution of magnetization in the trilayer can be determined by the condition that the free energy of the system is a minimum. The free energy is the sum of the exchange, the Zeeman, the magnetostatic, the magnetoelastic, and the anisotropy energies.[22] For trilayer systems,

the exchange energy consists of two parts; the interactions between neighboring atoms within each layer, and the long-range interlayer interactions between atoms in different layers. In Fig. 2 it can be seen that there are areas in which the moments in the two Co layers are aligned parallel throughout the magnetizing cycle, and areas in which the moments in the two Co layers are aligned antiparallel for certain values of applied field. The fact that the domain patterns seen in Figs. 2(a), 2(b), 2(c) and 2(d) are very similar to those seen in Figs. 2(e), 2(f), 2(g) and 2(h), respectively (except for a reversal of the magnetization directions), despite the fact that between these two images the applied magnetic field has been increased to saturation and then reduced, suggests that the magnetic domain configuration is closely related to the microstructure of the film.

The inhomogeneous way in which the magnetization of the film changes with applied field further suggests that the interlayer exchange coupling between the two Co layers is varying spatially. In the areas where the moments in the two layers remain parallel to each other in all applied fields, the interlayer exchange coupling is likely to be ferromagnetic, but the areas in which the magnetization switches to antiparallel in an applied field show a more complex behavior. It would normally be expected that antiferromagnetic coupling would lead to antiparallel alignment of the magnetic moments *in zero field*. In the trilayers studied in the present work, the antiparallel alignment does not occur in the remanent state, Figs. 2(a) and 2(e), but only after the application of a reverse field, Figs. 2(b) and 2(c), and 2(f) and 2(g). Two possible explanations can be suggested for the behavior observed in zero field. The first possibility is that the two Co layers are ferromagnetically coupled, but that local variations in microstructure lead to local variations in coercivity for one of the Co layers. The magnetization in the two Co layers would not reverse at the same value of applied field, resulting in regions of antiparallel aligned moments for certain values of applied field. The second possibility is that the coupling between the two Co layers varies across the film, but that the antiparallel alignment of the magnetization in the Co layers arising from the antiferromagnetic coupling is suppressed in the remanent state because of local pinning of the moments. The application of a reverse field allows the pinning energy to be overcome, resulting in the observed antiparallel alignment of the Co layers. In order to distinguish between these possibilities, the film was observed in an ac-demagnetized state. In this state, large areas of the film were found to show antiparallel alignment of the magnetization of the Co layers in zero field, showing that the second explanation for the observed behavior is likely to be the correct one. An image of such an area is shown in Fig. 4. If the film is then subjected to an applied magnetic field, the remanent state again shows only parallel alignment of the Co moments, with antiparallel alignment appearing only in nonzero fields.

Based on the current understanding of the factors that affect the interlayer exchange coupling in MLFs,[2] it is suggested that small variations in the Cr layer thickness are responsible for the change of the interlayer exchange coupling from ferromagnetic to antiferromagnetic from one area of the sample to another, and that the pinning of the moments is caused by the large number of grain boundaries and structural imperfections in the film.

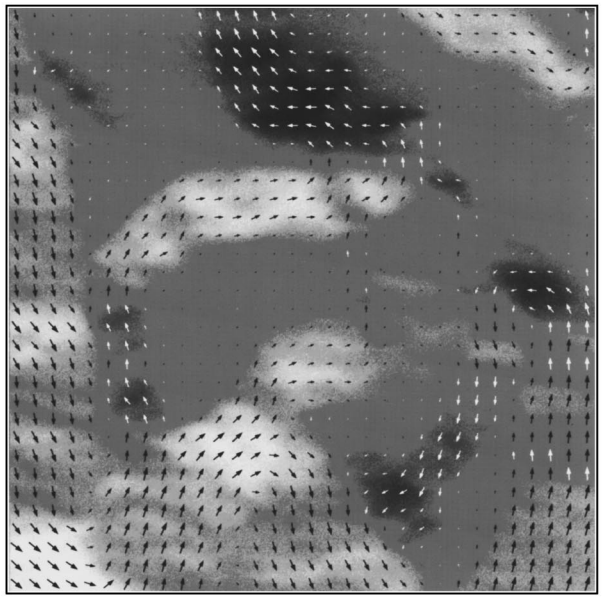

(a)

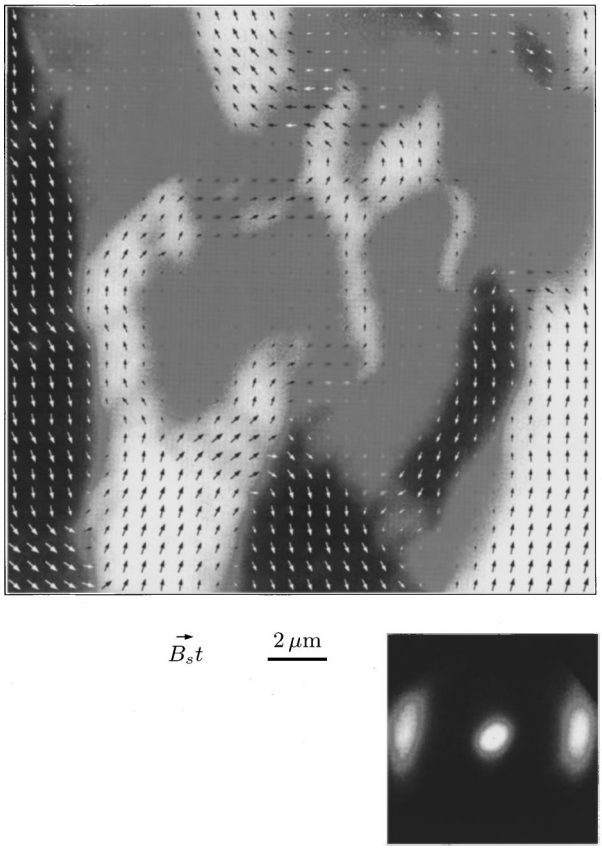

(b)

FIG. 4. Maps of $\mathbf{B}_i(x,y)$ for a different area of the same $Co_{10\,nm}/Cr_{1\,nm}/Co_{10\,nm}$ trilayer as shown in Figs. 1 and 2, in a demagnetized state. Maps of the components $B_{xi}(x,y)$ and $B_{yi}(x,y)$ are shown in (a) and (b), respectively. The arrow labeled B_st in (b) corresponds to $\mathbf{B}_i$ in a saturated region, and (b) also shows a high-magnification diffraction pattern.

The small distance over which the variations in the interlayer exchange coupling are observed is directly relevant to devices such as GMR read-heads, which are typically a few to a few tens of μm in size. This makes the mapping technique used in this work important for the study of these devices.

V. CONCLUSIONS

A recently developed Lorentz microscopy technique has been used to obtain maps of the magnetic induction from a sputter-deposited Co/Cr/Co trilayer at different points in its hysteresis cycle. The variation of the interlayer coupling in different parts of the specimen becomes evident after the application of a reverse field, rather than in the remanent state. This effect is due to local pinning of the magnetic moments in the remanent state. The results indicate the importance of studying local variations in interlayer coupling, for which our method is particularly suitable.

ACKNOWLEDGMENTS

The authors gratefully acknowledge the Engineering and Physical Sciences Research Council and the Royal Society for financial support. This work is part of an EU-funded collaboration (HCM Network on ''Magnetic Layered Structures''), and has been carried out within the framework of CAMST.

[1] M. N. Baibich, J. M. Broto, A. Fert, N. van Dau, and F. Petroff, Phys. Rev. Lett. **61**, 2472 (1988).
[2] S. S. P. Parkin, N. More, and K. P. Roche, Phys. Rev. Lett. **64**, 2304 (1990).
[3] D. M. Edwards, J. Mathon, and R. Bechara Muniz, IEEE Trans. Magn. **27**, 3548 (1991).
[4] R. L. White, IEEE Trans. Magn. **28**, 2482 (1992).
[5] J. Mathon, Contemp. Phys. **32**, 143 (1991).
[6] J. Unguris, R. J. Celotta, and D. T. Pierce, Phys. Rev. Lett. **67**, 140 (1991).
[7] S. T. Purcell, W. Folkerts, M. T. Johnson, N. W. E. McGee, K. Jager, J. A. de Stegge, W. B. Zeper, and W. Hoving, Phys. Rev. Lett. **67**, 903 (1991).
[8] A. C. Daykin and A. K. Petford-Long, Ultramicroscopy **58**, 365 (1995).
[9] A. C. Daykin and J. P. Jakubovics, J. Appl. Phys. **80**, 3408 (1996).
[10] H. W. Fuller and M. E. Hale, J. Appl. Phys. **31**, 238 (1960).
[11] J. P. Jakubovics, *Electron Microscopy in Materials Science*, edited by E. Ruedl and U. Valdrè (Commission of the European Communities, Brussels, 1975), Vol. IV, p. 1303.
[12] J. N. Chapman, J. Phys. D **17**, 623 (1984).
[13] H. W. Fuller and M. E. Hale, J. Appl. Phys. **31**, 1699 (1960).
[14] H. Boersch, H. Raith, and D. Wohlleben, Z. für Physik **159**, 388 (1960).
[15] R. P. Ferrier and R. T. Murray, Journal of the Royal Microscopical Society **85**, 323 (1966).
[16] W. J. S. Blackburn, G. H. Curtis, and R. P. Ferrier, J. Phys. E **2**, 570 (1969).
[17] N. H. Dekkers and H. de Lang, Optik (Stuttgart) **41**, 452 (1974).
[18] G. R. Morrison and J. N. Chapman, Optik (Stuttgart) **64**, 1 (1983).
[19] J. N. Chapman and G. R. Morrison, J. Magn. Magn. Mater. **35**, 254 (1983).
[20] J. N. Chapman, R. Ploessl, and D. M. Donnet, Ultramicroscopy **47**, 331 (1992).
[21] I. R. McFadyen, J. Appl. Phys. **64**, 6011 (1988).
[22] R. E. Camley and R. L. Stamps, J. Phys., Condens. Matter **5**, 3727 (1993).